

Polarization of the Cosmic Microwave Background

Mahsa Rahimi^a and Christian L. Reichardt^a

^aThe University of Melbourne, School of Physics, Parkville VIC 3010, Australia

© 2024 Elsevier Ltd. All rights reserved.

v 0.1

Nomenclature

CMB Cosmic microwave background

TES Transition edge sensor

Abstract

Since the first detection by the DASI experiment in 2002, measurements of the polarization of the cosmic microwave background (CMB) have grown into an important role in testing our understanding of conditions in the early universe and cosmology. The field has seen rapid experimental progress, driven in large part by the desire to make increasingly precise measurements of CMB polarization. Precise measurements of the CMB polarization anisotropies contain as much information as the CMB temperature anisotropy, and promise to unlock new tests of physics and the standard cosmological model.

In this chapter, we first discuss how polarization is produced through Thomson scattering, after which types of polarization patterns are connected to the cosmological sources. Finally, we briefly discuss the experimental hardware that enables these measurements.

Key points

- **Cosmic Microwave Background (CMB)** is 2.7 K black body radiation from the early Universe. The CMB radiation is partially polarized by Thomson scattering with electrons, giving rise to CMB polarization.
- **CMB anisotropies** are tiny spatial variations in the temperature and polarization patterns of the CMB radiation.
- **Thomson scattering** is elastic scattering between photons and a charged particle (generally electrons).
- **Radiation quadrupoles** are a radiation pattern with more intense incoming radiation on one axis, and less intense radiation on the perpendicular axis.
- **Inflation** is a period of accelerating expansion in the first moments of the Universe, during which the Universe is theorized to have expanded by a factor of $e^{60} - e^{100}$. Inflation is expected to produce density perturbations, which have been observed, and gravitational waves, which have yet to be observed.
- **Last scattering surface** is an image of the last time most CMB photons have scattered off matter. Last scattering occurs at recombination in the early Universe when the temperature cools enough for electrons and protons to recombine into neutral Hydrogen.
- **Linearly polarized** light has a preferred direction for the electric fields of the electromagnetic wave.
- **E-mode polarization** is a pattern of linear polarization which has zero curl. E-mode polarization is produced by acoustic waves in the CMB last scattering surface.
- **B-mode polarization** is a pattern of linear polarization which has zero gradient. B-mode polarization is produced by gravitational waves in the CMB last scattering surface.
- **Bolometers** are devices to measure radiative power through a temperature-dependent resistance.
- **Transition edge sensors (TESes)** are sensitive thermometers that utilize the sharp change in resistance as a superconductor transitions from normal to superconducting states.

1 Introduction

The cosmic microwave background (CMB) radiation is relic radiation from the hot plasma of the early Universe, some 400,000 years after the Big Bang. The CMB photons decoupled from electrons at recombination when the Universe had cooled sufficiently for the electron-proton plasma to combine to neutral hydrogen. This occurred at a temperature of 3000 K, with the subsequent expansion of the Universe by a factor of 1100 lowering the CMB temperature today to 2.72548 ± 0.00057 (Fixsen, 2009). As the scattering cross-section of hydrogen is small compared to the Thomson scattering cross-section of a free electron, the mean-free path of a photon increases precipitously during recombination. Most CMB photons have not scattered in the history of the Universe since recombination, which is also called the last scattering surface.

While scattering in a perfectly homogenous distribution of matter and photons does not create polarization, the early Universe is very slightly inhomogenous. In inflationary models, the initial perturbations are produced by quantum fluctuations in the inflationary field. These initial seeds then grow under the influence of gravity to the galaxies and large scale structure we see today. CMB anisotropy measurements provide a snapshot of the density perturbations at the last scattering surface.

Density (scalar) perturbations in the early hot plasma produce both temperature and polarization anisotropies in the CMB. As detailed in §2, the scattered light from a quadrupole radiation field scattering off a free electron will have a net linear polarization. The growth of quadrupole moments is suppressed while the photon mean free path is small, thus the resulting polarization patterns are more sensitive to physics occurring as the mean free path grows in the lead up to last scattering. Measuring polarization as well as temperature anisotropy roughly doubles the information content that can be extracted from CMB power spectrum measurements (Scott et al., 2016), and can break parameter degeneracies in some cosmological models (Galli et al., 2014). Precision measurements of CMB polarization can better

2 Polarization of the Cosmic Microwave Background

constrain physics of the early Universe, for instance by searching for possible new particles produced during the hot Big Bang (Abazajian and Kaplinghat, 2016). Additionally, by more tightly constraining starting conditions in the early Universe, CMB polarization measurements strengthen observational tests of the Universe’s late-time evolution.

The same situation also occurs in the late universe when light from the first stars and galaxies reionizes the Universe. The large-scale CMB quadrupole scatters off free electrons in the late Universe, adding additional polarization power at scales comparable to the horizon size at reionization. This “reionization bump” shows up at very large angular scales ($\ell \lesssim 10$) and measurements of the reionization bump by the WMAP and Planck satellites have been used to estimate the optical depth of the Universe to reionization (e.g., Hinshaw et al., 2013; Planck Collaboration et al., 2020b).

Finally, the standard model of cosmology includes a brief period of very rapid expansion in which the size of the Universe expands by a factor of $e^{60} - e^{100}$, called inflation. Models of inflation have made a number of successful predictions (Guth, 1981; Guth and Pi, 1982), such as that the Universe would be flat with a nearly scale-invariant power spectrum of initial density perturbations. The exponential expansion of the Universe during inflation is expected to produce a background of gravitational waves (tensor perturbations), which has not yet been observed. The power in these gravitational waves is related to the energy scale of inflation, and a detection (or upper limit) on these waves is one way to constrain the physics of inflation. The stretching and squeezing of spacetime at the last scattering surface by gravitational waves will also produce quadrupole radiation fields that scatter off the free electrons to produce linear polarization patterns. As discussed in §3, the symmetry of the polarization patterns produced by gravitational waves and density perturbations is different, so the physical origins of the observed polarization are distinguishable in principle. The search for these primordial gravitational waves from inflation has been described as a search for the “smoking gun of inflation”.

2 Generating CMB Polarization

The scattering mechanism between CMB photons and a plasma is Thomson scattering off the free electrons. Thomson scattering will produce linearly polarized light when the incident radiation field has a quadrupole moment. To understand the origin of polarization and when polarization is created, first consider a EM plane wave incident upon an electron from the $+x$ direction (see Fig. 1). The electron will oscillate in the $y - z$ plane. An observer in the $+z$ direction will see linearly polarized scattered light (in the y direction) since the electron does not move in x . This is over-simplified of course, as one would not expect all light to come from the same direction. In the case of an isotropic radiation field (Fig. 2), one has equal intensities of light impinging on the electron from all directions in the $x - y$ plane, and the electron oscillates in all directions equally. Thus the net linear polarization of scattered light would be zero since there is no preferred direction.

Now consider the case where there is a radiation quadrupole (Fig. 3). Without loss of generality, we can take the incoming radiation to have a higher intensity (higher temperature) in the $\pm y$ directions than in the $\pm x$ directions. The induced oscillations in the electron then will be larger on average along the x -direction than the y -direction. This causes the scattered light off the electron towards our observer in the $+z$ direction to be partially linearly polarized in the x -direction. An alternative way to understand this is that the differential cross-section of Thomson scattering, $\frac{d\sigma}{d\Omega}$, defined as the radiated intensity per solid angle $d\Omega$ over the incoming intensity per solid angle $d\Omega$, is proportional to the scalar product of the incident and scattered polarization vectors:

$$\frac{d\sigma}{d\Omega} = \frac{3\sigma_T}{8\pi} |\hat{\epsilon}' \cdot \hat{\epsilon}|^2, \quad (1)$$

where σ_T is the Thomson cross-section and the unit vectors $\hat{\epsilon}'$, $\hat{\epsilon}$ are aligned with the polarization direction in the incoming and outgoing light respectively. This means that the intensity of the scattered light peaks when the polarization of the incident and scattered light are parallel (For a pedagogical review, refer to Dodelson and Schmidt (2020), Hu and White (1997)). Importantly, Thomson scattering can not produce circular polarization. Thus the CMB is not expected to be circularly polarized, and most CMB experiments are insensitive to circular polarization. A larger quadrupole moment will increase the degree of linear polarization, with the scattered light 100% polarized when there is no incident light from the ‘cold’ directions. The CMB anisotropies are approximately 10% polarized due to this mechanism.

Well before recombination, photons are tightly coupled to the electrons of the plasma, and the photon mean free path between scattering is very short. With each scattering event, the photon direction is randomized which suppresses the growth of radiation quadrupoles. It is only near the last scattering surface that the photon mean free path lengthens sufficiently to allow quadrupole anisotropies to begin to grow. This is in contrast to the dark matter density perturbations which grow under the influence of gravity once a mode enters the horizon. Thus relative to the CMB temperature anisotropy, CMB polarization anisotropies are more sensitive to the details of what is happening around the time of recombination.

3 Sources of Polarization

As we have seen, quadrupole anisotropy in the radiation can yield polarized scattered light. In a spherical harmonics basis, a quadrupole corresponds to $\ell = 2$, which may have multipole values of $m = 0, 1, 2$. The different quadrupoles are produced by scalar (spin-0), vector and tensor (spin-2) perturbations respectively. Each type of quadrupole (and generating perturbation) yields a different polarization pattern and potential correlation between temperature and polarization.

Observationally, we have clear evidence for primordial density (scalar) perturbations in the Universe, as the density perturbations

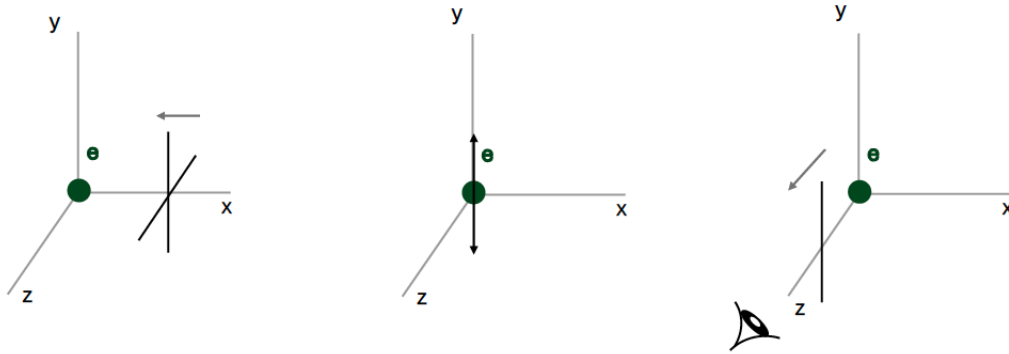


Fig. 1: The scattered light is polarized for Thomson scattering of light off a free electron. Left: Unpolarized light (no preferred direction for the electric field) is incident upon the electron from the $+x$ direction. Middle: The electromagnetic fields oscillate the electron in the plane perpendicular to propagation, here in the yz -plane. Viewed from the $+z$ -axis, the electron is only moving in $\pm y$. Right: An observer on the z -axis sees scattered light that is linearly polarized along the y -axis (illustration inspired from Hu and White (1997)).

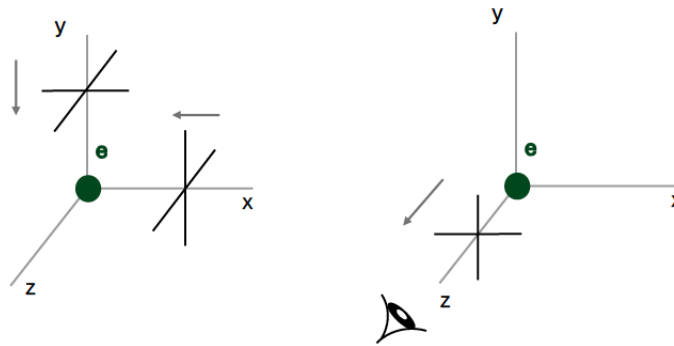


Fig. 2: For an isotropic distribution of light, the scattered light from Thomson scattering is unpolarized. Left: For an isotropic distribution of light, the incoming intensity from the $+x$ and $+y$ directions (or any other two directions separated by 90°) will be equal. Viewed by an observer along the z -axis, the electron will oscillate equally in the x and y directions. Right: Thus there will be no preferred direction for the electric field of the scattered light; the light is unpolarized. (illustration inspired from Hu and White (1997)).

are the seeds of all the structures we see in the Universe. We have not detected any direct evidence as yet for primordial vector or tensor (gravitational waves) perturbations. As noted earlier, inflationary models predict some level of primordial tensor perturbations (the inflationary gravitational waves).

Density (Scalar) Perturbations

One of the successes of CMB observations has been to measure the spectrum of primordial perturbations and show these initial conditions are consistent with a nearly-scale invariant power spectrum of density (scalar) perturbations. The tiny initial perturbations in density grow under the influence of gravity to produce first the CMB anisotropy and eventually all the structures we observe in the universe. Density perturbations can create the $m = 0$ version of a radiation quadrupole. Imagine an acoustic plane wave traveling in the y -direction perpendicular to the line of sight (\hat{z}) through the plasma, as in Fig. 4a. The passing wave will compress and rarify the plasma, creating a series of hot (denser) and cold (less dense) planes. An electron at a hot peak will see more radiation in the $\pm x$ directions and less radiation in the $\pm y$ directions, leading to linear polarization in the y -direction (parallel to the plane wave's direction of propagation). These directions are flipped for electrons at a cold peak, leading to linear polarization perpendicular to the plane wave's propagation direction. The local radiation field around an electron at the null of the wave is a gradient rather than a quadrupole, so there is no polarization at the nulls. Thus acoustic waves in the plasma will create polarization either parallel or perpendicular to the wave direction. It is also important to note that the largest polarization signal occurs at the peaks of the temperature signal, so scalar perturbations produce a non-zero correlation between the temperature and polarization anisotropies.

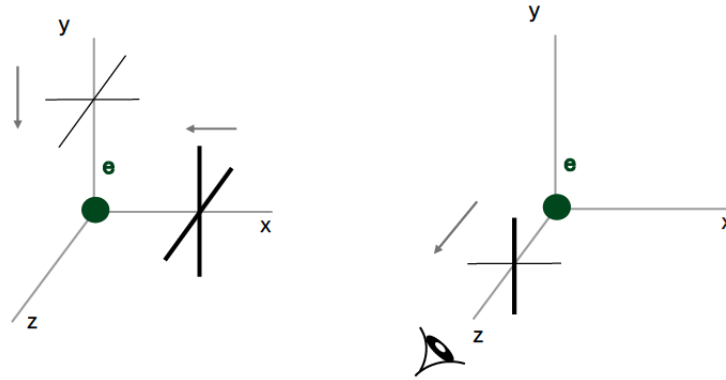


Fig. 3: A quadrupole radiation field generates linear polarization in the light scattered off a free electron. Left: A quadrupole radiation field means the light has a higher intensity (hotter) along one axis (taken to be the x-axis here), and lower intensity (cooler) on the perpendicular axis (here the y-axis). Right: Viewed by an observer along the z-axis, the electron's oscillations will be larger in the y-direction than x-direction. The electric field of the scattered light will tend to be larger in the y-direction, and the scattered light will be partially polarized (illustration inspired from Hu and White (1997)).

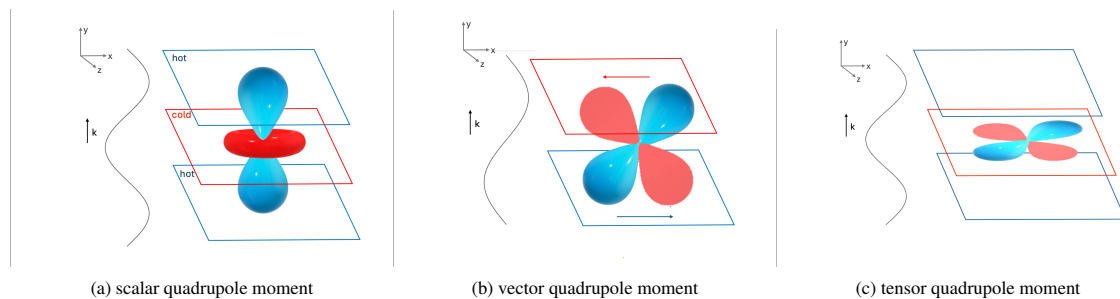


Fig. 4: The quadrupole moments of scalar (a), vector (b) and tensor (c) perturbations, representing $m = 0$, $m = 1$, $m = 2$ states of quadrupole, respectively. The blue/red planes represent the hot/cold or crest/trough planes of a single plane wave. The blue (red) lobes show the hot (cold) regions. The vectors point to the fluid velocity direction. Illustration adapted from Hu and White (1997).

Vorticity or Vector Perturbations

Vector perturbations represent vortical flows of matter, where the velocity field has a zero gradient and non-zero curl. A key difference to the last case is that while gravity amplifies scalar perturbations, any vector perturbations will decay in an expanding universe as the inverse square of the scale factor. Simple models of inflation do not produce vector perturbations, and even in more complicated inflationary scenarios the vector perturbations will have decayed away before recombination. However, observable vector perturbations may be generated in some models, for instance by topological defects near recombination. Note that while the vector perturbations will continue to decay away after recombination, their imprint (if any) on the CMB anisotropies would be preserved. Observational evidence for vector perturbations has not yet been uncovered.

We consider a single Fourier mode of the Fourier representation of the vector perturbations. In real space, this will generate velocity fields towards $\pm\hat{x}$ with magnitudes that vary along \hat{y} with the phase of the Fourier mode, as in Fig. 4b. We note that while this picture has been chosen to resemble the acoustic and gravitational waves in the left and right panels of the figure, vector perturbations do not satisfy a wave equation and do not oscillate unlike the other two cases. The direction of velocity reverses between each peak. An electron at the null will see a blueshift (hotter) then redshift (cooler) for the flow to the left above it, and a redshift (cooler) then blueshift (hotter) for the flow to the right below it. This quadrupole pattern corresponds to the $\ell = 2$, $m = 1$ multipole moment. The polarization produced will be largest at the nulls and at an angle $\pm 45^\circ$ to the wave direction.

Gravitational waves or Tensor Perturbations

Tensor perturbations, or gravitational waves, are distortions in the spacetime metric. A purely exponential expansion during inflation will lead to a scale-invariant initial power spectrum of these gravitational waves on super-horizon scales, and inflation models generically predict inflationary gravitational waves will exist with a nearly scale-invariant spectrum (Durrer, 2005). For historical reasons, the amplitude of the gravitational wave spectrum is parameterized as the ratio of the tensor to scalar power at some angular scale, normally called r . A major

thrust of current research is to search for these inflationary gravitational waves.

As a transverse wave, tensor perturbations compress and stretch the spacetime in directions perpendicular to the wave (see Fig. 4c). There are two possible polarizations of a gravitational wave, which we will label the + and \times polarizations. Consider a circular group of test particles with a gravitational wave propagating in the \hat{y} direction normal to the xz -plane of the circle. The + polarization alternately compresses and stretches the spacetime in horizontal and vertical directions causing the circle to be alternately elongated in top-to-bottom and side-to-side directions. The \times polarization distorts the spacetime in a 45° alignment with respect to the + polarization. The rarefaction and compression of the spacetime translates to redshift and blueshift of the photons in these directions, representing a temperature quadrupole moment with $\ell = 2, m = 2$, as shown in Figure 4c. The largest polarization signal will be seen by an observer whose line of sight is parallel to the wave direction.

4 Representations of CMB polarization

4.1 Stokes Parameters

The Stokes parameters, $\{I, Q, U, V = 0\}$, describe the intensity and polarization of light. The intensity I is the light's total intensity, while Q and U are measures of the light's linear polarization. V is a measure of the circular polarization of the radiation. As noted in §2, Thomson scattering does not produce circular polarization, so there should be no cosmological circular polarization. We expect $V = 0$ for the CMB, and will drop V for the remainder of the chapter.

The linear polarization parameters Q and U are the key parameters for CMB polarization. $Q > 0$ ($Q < 0$) represents polarization in the N-S (E-W) directions, while $V > 0$ ($V < 0$) refers to NE-SW (NW-SE) directions. Mathematically, considering the components of the electric field of the radiation along either the x/y axes (E_x, E_y) or the a/b axes (E_a, E_b) which are rotated 45° from the x/y axes, the Stokes parameters are

$$\begin{aligned} I &= |E_x|^2 + |E_y|^2 \\ &= |E_a|^2 + |E_b|^2, \\ Q &= |E_x|^2 - |E_y|^2, \\ U &= |E_a|^2 - |E_b|^2. \end{aligned} \quad (2)$$

One can define a complex vector, P , representing the total linear polarization:

$$P = Q + iU \quad (3)$$

which transforms like a spin-2 field under rotation (i.e. it is a double-sided arrow and by 180° rotation remains the same). The magnitude and angle of polarization are then defined as:

$$\begin{aligned} |P| &= \sqrt{Q^2 + U^2}, \\ \theta &= \frac{1}{2} \arctan\left(\frac{U}{Q}\right) \end{aligned} \quad (4)$$

with θ measured clockwise from the North direction.

It is important to note that these definitions are not invariant to rotations and changes to the local coordinate system. Specifically, if one rotates the axes by an angle ψ , the Q and U parameters will transform as:

$$\begin{aligned} Q' &= Q \cos 2\psi + U \sin 2\psi, \\ U' &= -Q \sin 2\psi + U \cos 2\psi, \end{aligned} \quad (5)$$

while the I parameter is unchanged. In CMB experiments, Stokes parameters are generally used when creating temperature and polarization maps from detectors where there are natural directions defined by the experiment's geometry.

4.2 E -modes and B -modes

For cosmological analyses, I, Q and U maps are generally converted to T, E and B maps, as these are (1) invariant under translations and rotations and (2) can be connected to the underlying physical sources of anisotropy. The polarization terms, E and B , are respectively a scalar (E) and pseudo-scalar (B) field (for more details, refer to Zaldarriaga (2001)). The nomenclature of E - and B -modes refers to the gradient-like and curl-like nature of the electric (E) and magnetic (B) fields. E -modes have a gradient and zero curl, while B -modes have zero gradient and non-zero curl. Alternatively, one can see the E - and B -modes are the parity eigenstates of polarization. E -modes have even parity (do not change sign under a parity transformation) while B -modes have odd parity (change sign under a parity transformation).

A full sky Q and U polarization map can be decomposed in spherical harmonic space using the spin-weighted spherical harmonics ${}_{\pm 2}Y_{\ell m}$ as:

$$(Q \pm iU)(\hat{n}) = \sum_{\ell} \sum_m (E_{\ell m} \pm iB_{\ell m}) {}_{\pm 2}Y_{\ell m}(\hat{n}) \quad (6)$$

The coefficients of this decomposition are the E - and B -modes. While the transformation from Q/U to E/B is invertible and linear on the full

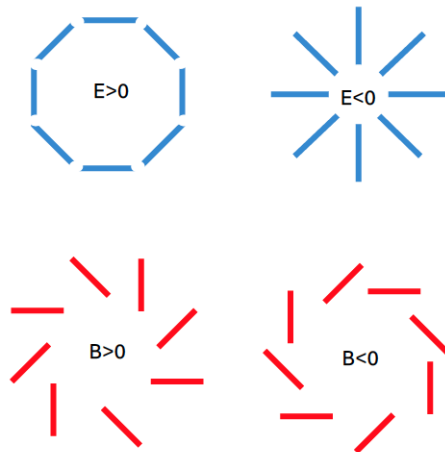


Fig. 5: The local polarization pattern near a positive or negative E -mode source (top), or a positive or negative B -mode source (bottom). The E -mode pattern is either tangential or radial around the source. As should be expected for even parity, the patterns are unchanged by taking a mirror image. The B -mode patterns are at 45° to the radial direction. Again given the odd parity, the B -mode pattern is not preserved when taking the mirror image.

sky, this transformation is non-local. Actual CMB experiments observe only part of the sky due to the Milky Way and/or the survey area, which can introduce confusion between E - and B - modes (read Smith (2006) for more discussion of this point and approaches to handle it).

For intuition, it is useful to consider what polarization patterns are represented by E and B modes. For E -modes, the polarization directions are either parallel or perpendicular to the gradient of the polarization magnitude (or wave direction). For B -modes, the polarization directions are $\pm 45^\circ$ to the gradient of the polarization magnitude. If one considers a location in the map with a high amplitude of E -modes, one will find a polarization pattern that is either tangential or radial around the point (see Fig. 5). In contrast, a location with a high amplitude of B -modes will show a corkscrew pattern around the point. The E -mode pattern shows mirror symmetry, while the B -mode pattern breaks mirror symmetry.

Beyond invariance to translations and rotations, using the E - and B -mode basis is convenient from a physics standpoint. Density perturbations at last scattering only produce T and E -modes. In the absence of vector or tensor perturbations, the CMB radiation field at last scattering will have zero B -modes. This is not true of generic polarization sources: gravitational waves, gravitational lensing, or polarized emission from the Milky Way all generate B -modes. As a result, one can separate the problems: measure density perturbations at last scattering with the CMB temperature and E -modes, while using B -modes to avoid the large sample variance due to density fluctuations while searching for gravitational waves or while measuring gravitational lensing.

CMB power spectra, C_ℓ^{XY} for $X, Y \in \{T, E, B\}$ have been the most important observable constraint from measurements of CMB anisotropy. We have not yet detected any non-Gaussianity in the primordial CMB perturbations, and the distribution of a Gaussian, statistically isotropic field can be fully described by:

$$\langle a_{\ell m}^X a_{\ell' m'}^Y \rangle = \delta_{\ell m} \delta_{\ell' m'} C_\ell^{XY} \quad (7)$$

The CMB power spectra are often reported in $D_\ell = \frac{\ell(\ell+1)}{2\pi} C_\ell$, as this quantity is nearly constant for a scale-invariant power spectrum. Note that the CMB spectra are expected to be zero for TB and EB ; the other four spectra (TT , TE , EE , BB) have been observationally measured at high signal-to-noise (see Fig. 6 for a compilation of recent measurements).

4.3 Temperature-Polarization Correlation

As acoustic waves in the early hot plasma produce both temperature and E -mode polarization anisotropies, it should be unsurprising that there are non-zero correlations between temperature and E -mode polarization. Measurements of the TE cross power spectrum are useful for consistency checks and as a source of complementary information to TT power spectrum measurements. Sources of astrophysical emissions are generally less polarized than the $\sim 10\%$ polarization of the CMB. Measurements of polarization, including the TE cross-power spectrum are thus less affected by possible foreground contamination especially at small angular scales (Couchot et al., 2017). This allows the CMB polarization power spectra to be measured to higher multipoles before foregrounds become important. The TE spectrum has been measured on a wide range of angular scales, from many-degrees to arcminute scales, with selected recent measurements shown in the lower panel of Fig. 6.

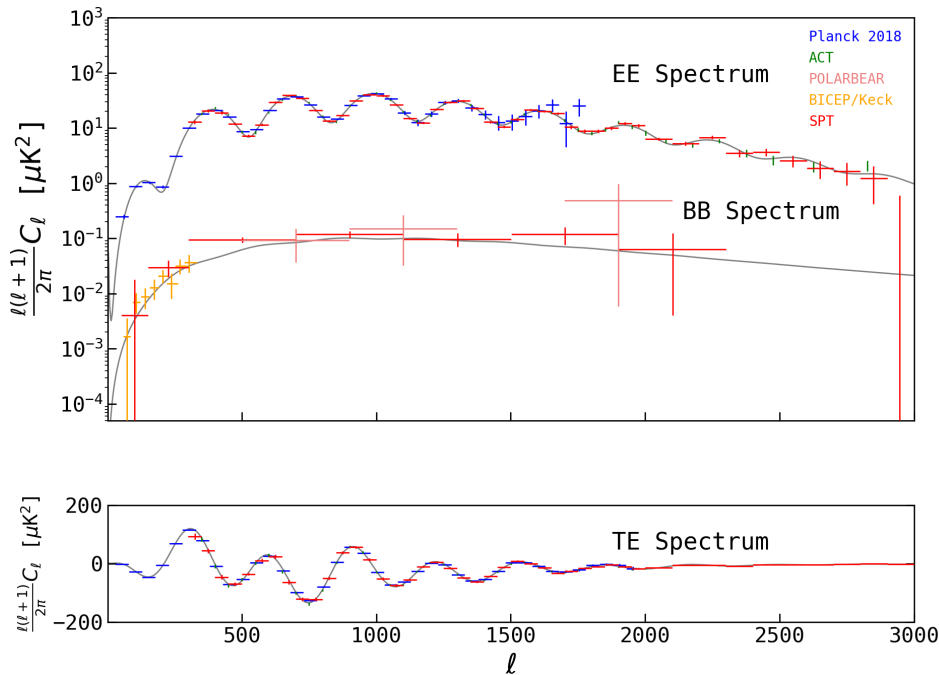


Fig. 6: Recent measurements of the CMB polarization power spectra from the Planck satellite (Planck Collaboration et al., 2020a), ACT (Choi et al., 2020), POLARBEAR (Adachi et al., 2020), and South Pole Telescope (SPT, Sayre et al. 2020; Dutcher et al. 2021) experiments. The E -mode auto-power spectrum, TE cross-power spectrum and B -mode auto-power spectrum have all been detected at high signal-to-noise.

5 Detecting CMB Polarization

The CMB polarization anisotropies have been measured from the ground, from balloons and from space. The first detection of CMB polarization was a 4.9σ detection of CMB E -mode power by the DASI experiment in 2002 (Kovac et al., 2002). The CMB B -modes created by gravitational lensing were first detected in 2013 at 7.7σ by cross-correlating B -modes measured by SPTpol with a B -mode template created using data from the SPIRE satellite and SPTpol (Hanson et al., 2013). An internal detection of lensing B -modes was first reported at 2.2σ in 2014 using the POLARBEAR experiment (Polarbear Collaboration et al., 2014). Today both the E - and B -mode power spectra have been measured at high significance by multiple experiments (see Fig. 6).

5.1 Observing frequencies and sites

Observations of CMB anisotropy reach the highest signal-to-noise at observing frequencies near 100-150 GHz (wavelengths 3 - 2 mm). This frequency range is also where the flux from the CMB is highest relative to the flux from other Galactic and extragalactic emission sources. Synchrotron (radio) emission falls with frequency while thermal dust emission rises with frequency. The optimal frequency range tends to be slightly lower for all-sky surveys compared to small-area surveys that are able to target regions with lower Galactic dust emission. Experiments also include detectors at other frequencies to leverage the different spectral energy distributions to disentangle the CMB anisotropy from the Galactic and extragalactic foreground emission.

Terrestrial telescopes must also deal with the Rayleigh-Jeans tail of thermal emission from the atmosphere. The main sources of atmospheric opacity include oxygen (mitigated by high elevation sites) and water vapor (mitigated by very dry and stable sites). These considerations motivate the two preeminent ground sites: the Atacama plateau at ~ 5000 m in Chile and the South Pole at ~ 3000 m in Antarctica. Atmospheric emission becomes a very significant source of noise at higher frequencies due to the ν^2 frequency scaling of the Rayleigh-Jeans tail and increasing atmospheric opacity (see Fig. 7). Space and balloon experiments above all or nearly all of the atmosphere have significant advantages in sensitivity per detector, especially as one moves towards larger angular scales or higher frequencies. However ground-based experiments can often accumulate significantly more detector-years of data. Most atmospheric emission is unpolarized, but polarization has been detected from the emission and scattering of atmospheric ice crystals (Takakura et al., 2019; Coerver et al., 2024).

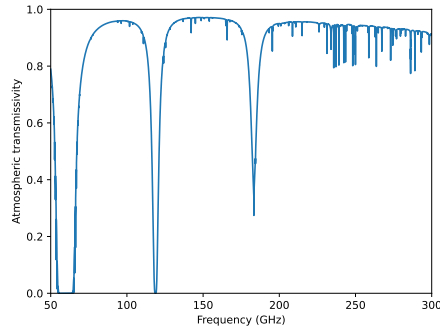


Fig. 7: Optical transmission through the atmosphere at the South Pole, estimated using the AM atmospheric model (Scott, 2023). The major absorption lines are due to water vapor (183 GHz) and molecular oxygen (60 and 118 GHz). These three lines explain why ground-based experiments typically define observing bands centered near 95 GHz, 150 GHz and 220 GHz. The Atacama plateau in Chile will have less oxygen (being higher elevation) and more water.

5.2 Common hardware elements to detect CMB polarization

While the design details vary, CMB polarization experiments all need to solve similar problems to measure the ultrafaint CMB polarization anisotropies against a background of instrumental noise, thermal emission from nearby warm objects (like the telescope mirrors), and astrophysical foregrounds. Each experiment generally includes the following elements:

- **Detectors.** Low noise detectors are critical to measuring the very faint CMB polarization anisotropy. The dominant detector technology is a bolometer (see §5.3), which uses a transition-edge sensor to measure the incoming optical power. At higher frequencies microwave kinetic inductance detectors (MKIDs) are sometimes used for their simpler fabrication. As one moves towards radio frequencies, interferometry becomes competitive for sensitivity.
- **Cryogenics.** Bolometers and MKIDs are operated at sub-Kelvin temperatures, as lower temperatures increase their sensitivity. Some detector noise terms (e.g., phonons, Johnson noise) increase with temperature. Active cooling is critical to achieve these temperatures. Additionally, cooling filters, lenses and other optical elements reduces the photon noise contribution from their thermal self-emission. Ground-based experiments use pulse-tube coolers (PTCs) to cool higher temperature stages (down to ~ 4 K). The PTCs work best when oriented vertically, which can impose operational constraints on observing elevations. For the detector stage, the field is transitioning from Helium sorption refrigerators which can achieve a few hundred mK with a duty cycle of order 70%, to more expensive dilution refrigerators which can provide continuous cooling to under 100 mK. Thus dilution refrigerators can increase observing time while reducing the detector noise levels. The Planck satellite demonstrated the first use of a dilution refrigerator in space.
- **Polarization-sensitive antennae.** This might be a dipole antenna (e.g., Austermann et al. 2012; POLARBEAR Collaboration et al. 2017), a phased array of dipole antennae (e.g., Ade et al. 2015), a sinuous wave antenna (e.g., Suzuki et al. 2016; Sobrin et al. 2022), among other possibilities. This allows the experiment to detect polarization.
- **(Optional) Polarization modulation.** Modulating the polarization signal through means such as a rotating half-wave plate (see highlighted box) can help with noise and the control of instrumental systematics. However, moving parts in the optical path have their own risks.

Half-wave plates

Certain crystalline materials, such as sapphire, are birefringent, meaning the material has a different index of refraction for linear polarizations of light depending on the orientation of the linear polarization to the crystalline structure. The birefringent properties of these crystals can be used to construct half-wave plates (HWPs) such that a phase shift of π is induced between the two polarization axes. This has the effect that if a linearly polarized plane wave enters the HWP polarized at an angle θ relative to the fast axis of the HWP, the linear polarization of the exiting wave will be at angle $-\theta$, a rotation of 2θ . HWPs in CMB experiments may be cooled to reduce their own thermal emission and include anti-reflection coatings to improve optical transmission. HWPs are used in CMB experiments to modulate the CMB polarization signal.

Signal modulation

A HWP rotating at frequency ν will rotate a static linear polarized source at 4ν , i.e. if the HWP is rotating at 1 Hz, a linearly polarized DC signal will now be modulated at 4 Hz. This can be useful for two reasons. First, it means both linear polarizations can be measured with the same detector, which can be useful for controlling instrumental systematic errors that can arise from differences between the properties of individual detectors. Second, it shifts the frequency range of the polarization signal to higher frequencies which reduces the penalty from low-frequency noise sources, such as atmospheric variability.

- **Lenses and mirrors.** These optical elements couple the antennae to the sky and set the size of the beam on the sky. Experiments targeting the inflationary gravitational wave signal, which can be done with degree-scale beams, frequently use cryogenically cooled lenses only. Other science goals benefit from few-arcminute-scale beams and include larger diameter mirrors in the optical design. Baffles and ground shields are frequently added to intercept stray light that might otherwise reach the detectors from the thermal emission of the warm ground.

- Filters. Filters are designed to allow some frequencies of light to pass while rejecting frequencies away from the desired signal band. Filters may achieve this rejection by absorption or reflection. Filters are needed for two reasons. First, blocking infrared light reduces the thermal load on the cryogenic system. This allows the detector and optical elements to be cooler (reducing their self-emission and thus contribution to the detector photon noise). Second, while the antenna are sensitive to a broad spectrum of photons, it is useful to define narrower observing frequency bands in order to leverage the different spectral energy distribution of the CMB versus foreground signals like thermal dust emission from the Milky Way to separate these signals.

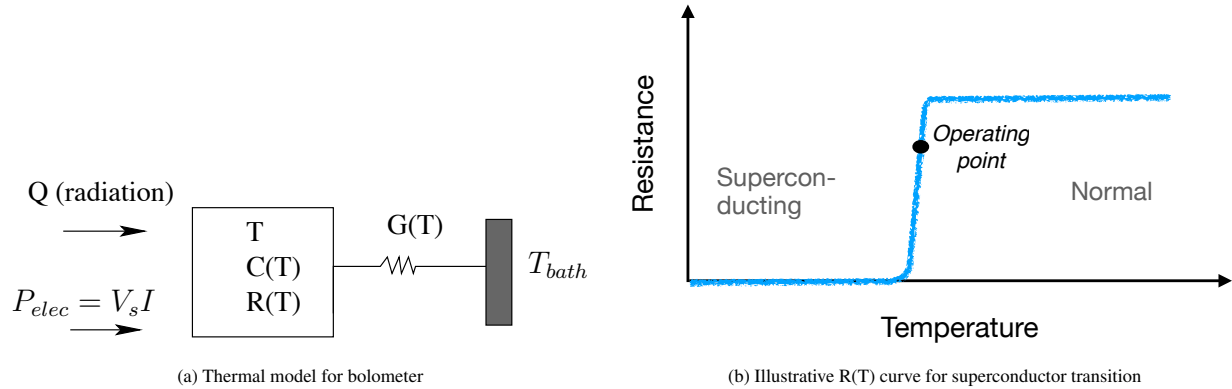


Fig. 8: *Left panel:* A simplified thermal model for a bolometer. The bolometer is heated to temperature T by the incoming power, a combination of radiative power Q and electrical power P_{elec} . At temperature T , the bolometer has a heat capacity $C(T)$ and resistivity $R(T)$. It is weakly thermally coupled with thermal conductance $G(T)$ to the bath at temperature T_{bath} . With electrical power P_{elec} fixed, the bolometer's temperature will increase when radiative power increases (and vice versa), in turn changing the resistance $R(T)$. *Right panel:* An illustrative diagram for the resistance as a function of temperature of a superconductor through the transition from superconducting to normal states. TES bolometers are operated at a temperature in the transition, marked by the black dot, where there is a very steep change in resistance with temperature. A SQUID amplifier is used to measure changes in the current flowing through the TES bolometer, which can be calibrated back to changes in incoming optical power.

5.3 Bolometers

Bolometers are designed to measure radiative power using a device with a temperature-dependent resistance. Bolometers are most sensitive when the resistance changes very quickly with temperature: the magnitude of dR/dT is large. The basic concept is illustrated in Fig. 8a. The bolometer absorbs radiation (Q) and electrical power (P_{elec}). In steady state, the incoming power is balanced by heat loss through the thermal link $G(T)$ to a colder base at T_{bath} . If the incoming power ($Q + P_{elec}$) increases, the bolometer temperature will increase and change its resistance $R(T)$. As a CMB telescope scans the sky, the small anisotropies in the CMB will translate to small variations in the bolometer temperature and resistance as a function of the telescope position and the detector's polarization angle.

While bolometers are the mainstay of CMB experiments today, many earlier experiments, including the DASI experiment that first detected CMB polarization and the WMAP satellite, used interferometric observations (Readhead and Pearson, 2004). Interferometry is still used at lower frequencies, including the low frequency instrument (LFI) on the Planck satellite. At higher frequencies, microwave kinetic inductance detectors (MKIDs) are beginning to compete with bolometers (Baselmans et al., 2017; Ulbricht et al., 2021). These other detector technologies become especially relevant for expanding the frequency range of observations to better discriminate between the CMB and astrophysical foregrounds (e.g. galactic synchrotron emission is brighter at low frequencies, while galactic dust dominates at high frequencies).

5.3.1 Neutron transmutation doped Germanium (NTD-Ge) bolometers

The first generation of bolometers that achieved photon-noise limited performance used semiconducting Germanium thermistors modified with neutron transmutation doping (NTD-Ge bolometers). These thermistors were suspended on silicon spiderwebs, strategically coated with gold to absorb light, placed behind feedhorns. The spiderweb structure allowed good absorption, possible polarization sensitivity, low thermal mass and a low cross-section to cosmic rays. CMB polarization experiments using these detectors include the first instrument of BICEP (ground), MAXIPOL (balloon), BOOMERanG (balloon), and the Planck satellite (space).

While individually sensitive, NTD-Ge bolometers are difficult to scale to larger detector arrays. The TES bolometers discussed next have three important advantages over the NTD-Ge bolometers. First, the NTD-Ge bolometers could not be lithographed as part of a monolithic array, but required assembly. Individually mounting thousands of NTD-Ge devices would be difficult and prone to poor yield. Second, NTD-Ge bolometers had very high impedance, as opposed to the $O(1) \Omega$ of TES bolometers. High impedance leads to a high sensitivity to microphonic noise, effectively requiring the use of liquid nitrogen and liquid helium instead of pulse tube cryocoolers. Serious microphonic

issues could also be created by vibrations from rotating half-wave plates or rapidly scanning telescopes. High impedance also ruled out the SQUID multiplexing techniques that can be used with TES bolometers. Individual wires for kilopixel arrays would conduct an unacceptably high thermal load onto the cold stages. These difficulties motivated the shift to TES bolometers.

5.3.2 Transition-edge sensor (TES) bolometers

Transition-edge sensor (TES) bolometers enabled experiments to grow from ~ 100 to 1000 detectors in the focal plane (see Fig. 9). TES bolometers are operated at a selected point (e.g. the black dot in the Fig. 8b) in a superconductor's transition from the superconducting state to normal state. The transition temperature of the device is chosen based on the expected optical power and bath temperature. As this transition happens over a very narrow range of temperatures, there can be a very large dR/dT in the transition even though the normal resistance is low enough to avoid issues with microphonics. TES bolometers are voltage biased to operate at a specific resistance, e.g. $0.7R_N$ for 70% of the normal resistance R_N . When the optical power increases, the electrical power decreases to hold stable the TES resistance (and temperature). The optical power falling on the bolometer is inferred from the required electrical power, which is read out by means of a SQUID amplifier. SQUIDs are very sensitive magnetometers that can be used to measure current. Multiplexing (reading out multiple detectors on a single wire to the cold stages) can be achieved by either biasing individual detectors at different frequencies, by reading out detectors at different times, or a combination of both temporal and frequency multiplexing (Irwin et al., 2010). Some examples of CMB polarization experiments using multiplexed TES bolometers include SPT-3G (ground), BICEP3 (ground), Simons Observatory (ground), and SPIDER (balloon) (Sobrin et al., 2022; Moncelsi et al., 2020; McCarrick et al., 2021; Gualtieri et al., 2018). Designs for future experiments such as CMB-S4 (ground, 2030) and LiteBIRD (space, 2032) also include TES bolometers (Matsumura et al., 2016; Abitbol et al., 2017).

5.4 Future technology directions

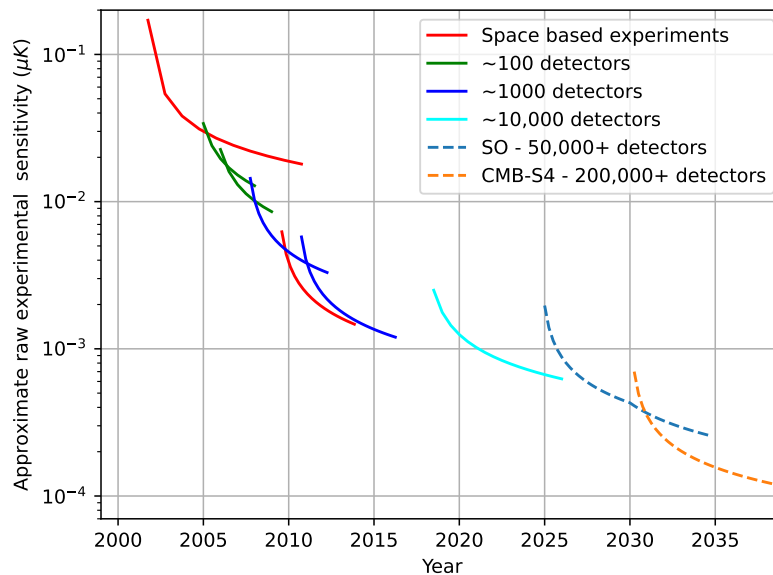


Fig. 9: Progress in raw experimental sensitivity over time. Driven by the ability to construct and field larger detector arrays, the field has seen sensitivity improving at near-exponential rates with time. The red lines are for the WMAP and Planck satellites. The green, blue, and cyan lines are for selected ground-based experiments with $O(100)$, $O(1000)$, and $O(10,000)$ detectors respectively. The dashed blue line is for the Simons Observatory in Chile, which is taking engineering data in 2024, and has a funded upgrade to approximately double the detector count midway through the 10-year survey. The dashed orange line is for the planned CMB-S4 experiment, which will observe for an estimated 10 years from Chile and possibly the South Pole.

As the sensitivity of individual CMB detectors has been limited for some time by the fundamental noise floor set by the randomness of photons arriving at the detector, much effort has been devoted to building receivers with ever increasing numbers of detectors. This has led to a version of “Moore’s law” showing near exponential growth in CMB detector counts with time (see Fig. 9). The continued drive for more detectors has necessitated progress on a number of related technological fronts, such as:

1. Improving the yield percentage and repeatability on the nanofabrication process of detectors.
2. Redesigning the telescope optics to increase the focal plane area (allowing more detectors on the same telescope).

3. Increasing the maximum manufacturable size for optical filters, lenses, and their anti-reflection coatings (again allowing larger focal plans).
4. Improvements to the detector readout electronics, including work to reduce readout noise, to improve the ease and reliability of biasing detectors, and to increase the multiplexing factor and thus reduce the thermal load on the cryogenic system.

Very active technological development programs have been crucial to enable each generation of CMB experiment to be noticeably more sensitive.

6 Conclusions

Observations of CMB polarization anisotropies are increasingly important to our understanding of the universe. Upcoming measurements of CMB polarization anisotropies present opportunities to detect inflationary gravitational waves, to discover new light particles produced during the Big Bang, and test the standard model of cosmology.

Acknowledgments

We thank Jessica Zebrowski, Justin Clancy, Nicholas Huang, Srinivasan Raghunathan, Junhao Zhan, and Michael Doohan for the valuable feedback they provided on the draft.

References

- Abazajian KN and Kaplinghat M (2016). Neutrino physics from the cosmic microwave background and large-scale structure. *Annual Review of Nuclear and Particle Science* 66 (Volume 66, 2016): 401–420. ISSN 1545-4134. doi:<https://doi.org/10.1146/annurev-nucl-102014-021908>. <https://www.annualreviews.org/content/journals/10.1146/annurev-nucl-102014-021908>, Journal Article.
- Abitbol MH, Ahmed Z, Barron D, Basu Thakur R, Bender AN, Benson BA, Bischoff CA, Bryan SA, Carlstrom JE, Chang CL, Chuss DT, Crowley KT, Cukierman A, de Haan T, Dobbs M, Essinger-Hileman T, Filippini JP, Ganga K, Gudmundsson JE, Halverson NW, Hanany S, Henderson SW, Hill CA, Ho SPP, Hubmayr J, Irwin K, Jeong O, Johnson BR, Kernasovskiy SA, Kovac JM, Kusaka A, Lee AT, Maria S, Mauskopf P, McMahon JJ, Moncelsi L, Nadolski AW, Nagy JM, Niemack MD, O'Brien RC, Padin S, Parshley SC, Pryke C, Roe NA, Rostem K, Ruhl J, Simon SM, Staggs ST, Suzuki A, Switzer ER, Tajima O, Thompson KL, Timbie P, Tucker GS, Vieira JD, Vieregg AG, Westbrook B, Wollack EJ, Yoon KW, Young KS and Young EY (2017), Jun. CMB-S4 Technology Book, First Edition. *arXiv e-prints*, arXiv:1706.02464doi: 10.48550/arXiv.1706.02464. 1706.02464.
- Adachi S, Aguilar Faúndez MAO, Arnold K, Baccigalupi C, Barron D, Beck D, Bianchini F, Chapman S, Cheung K, Chinone Y, Crowley K, Dobbs M, Bouhargani HE, Elleflot T, Errard J, Fabbian G, Feng C, Fujino T, Galitzki N, Goeckner-Wald N, Groh J, Hall G, Hasegawa M, Hazumi M, Hirose H, Jaffe AH, Jeong O, Kaneko D, Katayama N, Keating B, Kikuchi S, Kisner T, Kusaka A, Lee AT, Leon D, Linder E, Lowry LN, Matsuda F, Matsumura T, Minami Y, Navaroli M, Nishino H, Pham ATP, Poletti D, Reichardt CL, Segawa Y, Siritanasak P, Tajima O, Takakura S, Takatori S, Tanabe D, Tepy GP, Tsai C, Vergès C, Westbrook B and Zhou Y (2020), Nov. A measurement of the cmb e-mode angular power spectrum at subdegree scales from 670 square degrees of polarbear data. *The Astrophysical Journal* 904 (1): 65. ISSN 1538-4357. doi:10.3847/1538-4357/abbacd. <http://dx.doi.org/10.3847/1538-4357/abbacd>.
- Ade PAR, Aikin RW, Amiri M, Barkats D, Benton SJ, Bischoff CA, Bock JJ, Bonetti JA, Brevik JA, Buder I, Bullock E, Chattopadhyay G, Davis G, Day PK, Dowell CD, Duband L, Filippini JP, Fliescher S, Golwala SR, Halpern M, Hasselfield M, Hildebrandt SR, Hilton GC, Hristov V, Hui H, Irwin KD, Jones WC, Karkare KS, Kaufman JP, Keating BG, Kefeli S, Kernasovskiy SA, Kovac JM, Kuo CL, LeDuc HG, Leitch EM, Llombart N, Lueker M, Mason P, Moncelsi L, Netterfield CB, Nguyen HT, O'Brien R, IV RWO, Orlando A, Pryke C, Rahlin AS, Reintsema CD, Richter S, Runyan MC, Schwarz R, Sheehy CD, Staniszewski ZK, Sudiwala RV, Tepy GP, Tolan JE, Trangsrud A, Tucker RS, Turner AD, Vieregg AG, Weber A, Wiebe DV, Wilson P, Wong CL, Yoon KW, Zmuidzinas J and for the Bicep2, Keck Array, and Spider Collaborations (2015), oct. Antenna-coupled tes bolometers used in bicep2, keck array, and spider. *The Astrophysical Journal* 812 (2): 176. doi:10.1088/0004-637X/812/2/176. <https://dx.doi.org/10.1088/0004-637X/812/2/176>.
- Austermann JE, Aird KA, Beall JA, Becker D, Bender A, Benson BA, Bleem LE, Britton J, Carlstrom JE, Chang CL, Chiang HC, Cho HM, Crawford TM, Crites AT, Datesman A, de Haan T, Dobbs MA, George EM, Halverson NW, Harrington N, Henning JW, Hilton GC, Holder GP, Holzappel WL, Hoover S, Huang N, Hubmayr J, Irwin KD, Keisler R, Kennedy J, Knox L, Lee AT, Leitch E, Li D, Lueker M, Marrone DP, McMahon JJ, Mehl J, Meyer SS, Montroy TE, Natoli T, Nibarger JP, Niemack MD, Novosad V, Padin S, Pryke C, Reichardt CL, Ruhl J, Saliwanchik BR, Sayre JT, Schaffer KK, Shirokoff E, Stark AA, Story K, Vanderlinde K, Vieira JD, Wang G, Williamson R, Yefremenko V, Yoon KW and Zahn O (2012), Sep., SPTpol: an instrument for CMB polarization measurements with the South Pole Telescope, Holland WS and Zmuidzinas J, (Eds.), Millimeter, Submillimeter, and Far-Infrared Detectors and Instrumentation for Astronomy VI, Society of Photo-Optical Instrumentation Engineers (SPIE) Conference Series, 8452, pp. 84521E, 1210. 4970.
- Baselmans JJA, Bueno J, Yates SJC, Yurduseven O, Llombart N, Karatsu K, Baryshev AM, Ferrari L, Endo A, Thoen DJ, de Visser PJ, Janssen RMJ, Murugesan V, Driessen EFC, Coiffard G, Martin-Pintado J, Hargrave P and Griffin M (2017), May. A kilo-pixel imaging system for future space based far-infrared observatories using microwave kinetic inductance detectors. *A&A* 601, A89. doi:10.1051/0004-6361/201629653. 1609.01952.
- Choi SK, Hasselfield M, Ho SPP, Koopman B, Lungu M, Abitbol MH, Addison GE, Ade PAR, Aiola S, Alonso D, Amiri M, Amodeo S, Angile E, Austermann JE, Baidon T, Battaglia N, Beall JA, Bean R, Becker DT, Bond JR, Bruno SM, Calabrese E, Calafut V, Campusano LE, Carrero F, Chesmore GE, Cho Hm, Clark SE, Cothard NF, Crichton D, Crowley KT, Darwish O, Datta R, Denison EV, Devlin MJ, Duell CJ, Duff SM, Duivenvoorden AJ, Dunkley J, Dünner R, Essinger-Hileman T, Fankhanel M, Ferraro S, Fox AE, Fuzia B, Gallardo PA, Gluscevic V, Golec JE, Grace E, Gralla M, Guan Y, Hall K, Halpern M, Han D, Hargrave P, Henderson S, Hensley B, Hill JC, Hilton GC, Hilton M, Hincks AD, Hložek R, Hubmayr J, Huppenberger KM, Hughes JP, Infante L, Irwin K, Jackson R, Klein J, Knowles K, Kosowsky A, Lakey V, Li D, Li Y, Li Z, Lokken M, Louis T, MacInnis A, Madhavacheril M, Maldonado F, Mallaby-Kay M, Marsden D, Maurin L, McMahon J, Menanteau F, Moodley K, Morton T, Naess S, Namikawa T, Nati F, Newburgh L, Nibarger JP, Nicola A, Niemack MD, Nolte MR, Orłowski-Sherer J, Page LA, Pappas CG, Partridge

- B, Phakathi P, Prince H, Puddu R, Qu FJ, Rivera J, Robertson N, Rojas F, Salatino M, Schaan E, Schillaci A, Schmitt BL, Sehgal N, Sherwin BD, Sierra C, Sievers J, Sifon C, Sikhosana P, Simon S, Spergel DN, Staggs ST, Stevens J, Storer E, Sunder DD, Switzer ER, Thorne B, Thornton R, Trac H, Treu J, Tucker C, Vale LR, Van Engelen A, Van Lanen J, Vavagiakis EM, Wagoner K, Wang Y, Ward JT, Wollack EJ, Xu Z, Zago F and Zhu N (2020), Dec. The Atacama Cosmology Telescope: a measurement of the Cosmic Microwave Background power spectra at 98 and 150 GHz. *JCAP* 2020 (12), 045. doi:10.1088/1475-7516/2020/12/045. 2007.07289.
- Coerver A, Zebrowski JA, Takakura S, Holzapfel WL, Ade PAR, Anderson AJ, Ahmed Z, Ansarinejad B, Archipley M, Balkenhol L, Barron D, Benabed K, Bender AN, Benson BA, Bianchini F, Bleem LE, Bouchet FR, Bryant L, Camphuis E, Carlstrom JE, Cecil TW, Chang CL, Chaubal P, Chichura PM, Chokshi A, Chou TL, Crawford TM, Cukierman A, Daley C, de Haan T, Dibert KR, Dobbs MA, Doussot A, Dutcher D, Everett W, Feng C, Ferguson KR, Fichman K, Foster A, Galli S, Gambrel AE, Gardner RW, Ge F, Goeckner-Wald N, Gualtieri R, Guidi F, Guns S, Halverson NW, Hivon E, Holder GP, Hood JC, Hryciuk A, Huang N, Keruzore F, Khalife AR, Knox L, Korman M, Kornoele K, Kuo CL, Lee AT, Levy K, Lowitz AE, Lu C, Maniyar A, Martsen ES, Menanteau F, Millea M, Montgomery J, Nakato Y, Natoli T, Noble GI, Novosad V, Omori Y, Padin S, Pan Z, Paschos P, Phadke KA, Pollak AW, Prabhu K, Quan W, Rahimi M, Rahlin A, Reichardt CL, Rouble M, Ruhl JE, Schiappucci E, Smecher G, Sobrin JA, Stark AA, Stephen J, Suzuki A, Tandoi C, Thompson KL, Thorne B, Trendafilova C, Tucker C, Umlita C, Vieira JD, Vitrier A, Wan Y, Wang G, Whitehorn N, Wu WLK, Yefremenko V and Young MR (2024), Jul. Measurement and Modeling of Polarized Atmosphere at the South Pole with SPT-3G. *arXiv e-prints*, arXiv:2407.20579doi:10.48550/arXiv.2407.20579. 2407.20579.
- Couchot F, Henrot-Versillé S, Perdureau O, Plaszczynski S, Rouillé d'Orfeuil B, Spinelli M and Tristram M (2017), Jun. Cosmology with the cosmic microwave background temperature-polarization correlation. *A&A* 602, A41. doi:10.1051/0004-6361/201629815. 1609.09730.
- Dodelson S and Schmidt F (2020). *Modern Cosmology*. doi:10.1016/C2017-0-01943-2.
- Durrer R (2005), *Cosmological Perturbation Theory*, Papantonopoulos E, (Ed.), *The Physics of the Early Universe*, 653, pp. 31.
- Dutcher D, Balkenhol L, Ade PAR, Ahmed Z, Anderes E, Anderson AJ, Archipley M, Avva JS, Aylor K, Barry PS, Basu Thakur R, Benabed K, Bender AN, Benson BA, Bianchini F, Bleem LE, Bouchet FR, Bryant L, Byrum K, Carlstrom JE, Carter FW, Cecil TW, Chang CL, Chaubal P, Chen G, Cho HM, Chou TL, Cliche JF, Crawford TM, Cukierman A, Daley C, de Haan T, Denison EV, Dibert K, Ding J, Dobbs MA, Everett W, Feng C, Ferguson KR, Foster A, Fu J, Galli S, Gambrel AE, Gardner RW, Goeckner-Wald N, Gualtieri R, Guns S, Gupta N, Guysier R, Halverson NW, Harke-Hosemann AH, Harrington NL, Henning JW, Hilton GC, Hivon E, Holder GP, Holzapfel WL, Hood JC, Howe D, Huang N, Irwin KD, Jeong OB, Jonas M, Jones A, Khaire TS, Knox L, Kofman AM, Korman M, Kubik DL, Kuhlmann S, Kuo CL, Lee AT, Leitch EM, Lowitz AE, Lu C, Meyer SS, Michalik D, Millea M, Montgomery J, Nadolski A, Natoli T, Nguyen H, Noble GI, Novosad V, Omori Y, Padin S, Pan Z, Paschos P, Pearson J, Posada CM, Prabhu K, Quan W, Raghunathan S, Rahlin A, Reichardt CL, Riebel D, Riedel B, Rouble M, Ruhl JE, Sayre JT, Schiappucci E, Shirokoff E, Smecher G, Sobrin JA, Stark AA, Stephen J, Story KT, Suzuki A, Thompson KL, Thorne B, Tucker C, Umlita C, Vale LR, Vanderlinde K, Vieira JD, Wang G, Whitehorn N, Wu WLK, Yefremenko V, Yoon KW, Young MR and SPT-3G Collaboration (2021), Jul. Measurements of the E-mode polarization and temperature-E-mode correlation of the CMB from SPT-3G 2018 data. *PRD* 104 (2), 022003. doi:10.1103/PhysRevD.104.022003. 2101.01684.
- Fixsen DJ (2009), Dec. The Temperature of the Cosmic Microwave Background. *ApJ* 707 (2): 916–920. doi:10.1088/0004-637X/707/2/916. 0911.1955.
- Galli S, Benabed K, Bouchet Fmc, Cardoso JFmc, Elsner F, Hivon E, Mangilli A, Prunet S and Wandelt B (2014), Sep. Cmb polarization can constrain cosmology better than cmb temperature. *Phys. Rev. D* 90: 063504. doi:10.1103/PhysRevD.90.063504. <https://link.aps.org/doi/10.1103/PhysRevD.90.063504>.
- Gualtieri R, Filippini JP, Ade PAR, Amiri M, Benton SJ, Bergman AS, Bihary R, Bock JJ, Bond JR, Bryan SA, Chiang HC, Contaldi CR, Doré O, Duivenvoorden AJ, Eriksen HK, Farhang M, Fissel LM, Fraise AA, Freese K, Galloway M, Gambrel AE, Gandilo NN, Ganga K, Gramillano RV, Gudmundsson JE, Halpern M, Hartley J, Hasselfield M, Hilton G, Holmes W, Hristov VV, Huang Z, Irwin KD, Jones WC, Kuo CL, Kermish ZD, Li S, Mason PV, Megerian K, Moncelsi L, Morford TA, Nagy JM, Netterfield CB, Nolte M, Osherson B, Padilla IL, Racine B, Rahlin AS, Reintsema C, Ruhl JE, Runyan MC, Ruud TM, Shariff JA, Soler JD, Song X, Trangsrud A, Tucker C, Tucker RS, Turner AD, List JFvd, Weber AC, Wehus IK, Wiebe DV and Young EY (2018), Dec. SPIDER: CMB Polarimetry from the Edge of Space. *Journal of Low Temperature Physics* 193 (5-6): 1112–1121. doi:10.1007/s10909-018-2078-x. 1711.10596.
- Guth AH (1981), Jan. Inflationary universe: A possible solution to the horizon and flatness problems. *PRD* 23: 347–356.
- Guth AH and Pi S (1982), Oct. Fluctuations in the new inflationary universe. *PRL* 49: 1110–1113.
- Hanson D, Hoover S, Crites A, Ade PAR, Aird KA, Austermann JE, Beall JA, Bender AN, Benson BA, Bleem LE, Bock JJ, Carlstrom JE, Chang CL, Chiang HC, Cho HM, Conley A, Crawford TM, de Haan T, Dobbs MA, Everett W, Gallicchio J, Gao J, George EM, Halverson NW, Harrington N, Henning JW, Hilton GC, Holder GP, Holzapfel WL, Hrubes JD, Huang N, Hubmayr J, Irwin KD, Keisler R, Knox L, Lee AT, Leitch E, Li D, Liang C, Luong-Van D, Marsden G, McMahan JJ, Mehl J, Meyer SS, Moczul L, Montroy TE, Natoli T, Nibarger JP, Novosad V, Padin S, Pryke C, Reichardt CL, Ruhl JE, Saliwanchik BR, Sayre JT, Schaffer KK, Schulz B, Smecher G, Stark AA, Story KT, Tucker C, Vanderlinde K, Vieira JD, Viero MP, Wang G, Yefremenko V, Zahn O and Zemcov M (SPTpol Collaboration) (2013), Sep. Detection of b-mode polarization in the cosmic microwave background with data from the south pole telescope. *PRL* 111: 141301. doi:10.1103/PhysRevLett.111.141301. <https://link.aps.org/doi/10.1103/PhysRevLett.111.141301>.
- Hinshaw G, Larson D, Larson D, Bennett CL, Dunkley J, Nolte MR, Halpern M, Hill RS, Odegard N, Page L, Smith KM, Weiland JL, Gold B, Jarosik N, Kogut A, Limon M, Meyer SS, Tucker GS, Wollack E and Wright EL (2013), Oct. Nine-year Wilkinson Microwave Anisotropy Probe (WMAP) Observations: Cosmological Parameter Results. *ApJS* 208 (2), 19. doi:10.1088/0067-0049/208/2/19. 1212.5226.
- Hu W and White M (1997), Oct. A CMB polarization primer. *New Astronomy* 2 (4): 323–344. doi:10.1016/S1384-1076(97)00022-5. astro-ph/9706147.
- Irwin KD, Niemack MD, Beyer J, Cho HM, Doriese WB, Hilton GC, Reintsema CD, Schmidt DR, Ullom JN and Vale LR (2010), Mar. Code-division multiplexing of superconducting transition-edge sensor arrays. *Superconductor Science Technology* 23 (3), 034004. doi:10.1088/0953-2048/23/3/034004.
- Kovac JM, Leitch EM, Pryke C, Carlstrom JE, Halverson NW and Holzapfel WL (2002), Dec. Detection of polarization in the cosmic microwave background using DAS1. *Nature* 420 (6917): 772–787. doi:10.1038/nature01269. astro-ph/0209478.
- Matsumura T, Akiba Y, Arnold K, Borrill J, Chandra R, Chinone Y, Cukierman A, de Haan T, Dobbs M, Dominjon A, Elleflot T, Errard J, Fujino T, Fuke H, Goeckner-wald N, Halverson N, Harvey P, Hasegawa M, Hattori K, Hattori M, Hazumi M, Hill C, Hilton G, Holzapfel W, Hori Y, Hubmayr J, Ichiki K, Inatani J, Inoue M, Inoue Y, Irie F, Irwin K, Ishino H, Ishitsuka H, Jeong O, Karatsu K, Kashima S, Katayama N, Kawano I, Keating B, Kibayashi A, Kibe Y, Kida Y, Kimura K, Kimura N, Kohri K, Komatsu E, Kuo CL, Kuromiya S, Kusaka A, Lee A, Linder E, Matsuhara H, Matsuoka S, Matsuura S, Mima S, Mitsuda K, Mizukami K, Morii H, Morishima T, Nagai M, Nagasaki T, Nagata R, Nakajima M, Nakamura S, Namikawa T, Naruse M, Natsume K, Nishibori T, Nishijo K, Nishino H, Nitta T, Noda A, Noguchi T, Ogawa H, Oguri S, Ohta IS, Otani C, Okada N, Okamoto A, Okamoto A, Okamura T, Rebeiz G, Richards P, Sakai S, Sato N, Sato Y, Segawa Y, Sekiguchi S, Sekimoto Y, Sekine M, Seljak U, Sherwin B, Shinozaki K, Shu S, Stompor R, Sugai H, Sugita H, Suzuki T, Suzuki A, Tajima O, Takada S, Takakura S, Takano K, Takei Y, Tomaru T, Tomita N, Turin P, Utsunomiya S, Uzawa Y, Wada T, Watanabe H, Westbrook B, Whitehorn N, Yamada Y, Yamasaki N, Yamashita T, Yoshida M, Yoshida T and Yotsumoto Y (2016), Aug. LiteBIRD: Mission Overview and Focal Plane Layout. *Journal of Low*

- Temperature Physics* 184 (3-4): 824–831. doi:10.1007/s10909-016-1542-8.
- McCarrick H, Healy E, Ahmed Z, Arnold K, Atkins Z, Austermann JE, Bhandarkar T, Beall JA, Bruno SM, Choi SK, Connors J, Cothard NF, Crowley KD, Dicker S, Dober B, Duell CJ, Duff SM, Dutcher D, Frisch JC, Galitzki N, Gralla MB, Gudmundsson JE, Henderson SW, Hilton GC, Ho SPP, Huber ZB, Hubmayr J, Iuliano J, Johnson BR, Kofman AM, Kusaka A, Lashner J, Lee AT, Li Y, Link MJ, Lucas TJ, Lungu M, Mates JAB, McMahon JJ, Niemack MD, Orłowski-Scherer J, Seibert J, Silva-Feaver M, Simon SM, Staggs S, Suzuki A, Terasaki T, Thornton R, Ullom JN, Vavagiakis EM, Vale LR, Van Lanen J, Vissers MR, Wang Y, Wollack EJ, Xu Z, Young E, Yu C, Zheng K and Zhu N (2021), Nov. The Simons Observatory Microwave SQUID Multiplexing Detector Module Design. *ApJ* 922 (1), 38. doi:10.3847/1538-4357/ac2232. 2106.14797.
- Moncelsi L, Ade PAR, Ahmed Z, Amiri M, Barkats D, Basu Thakur R, Bischoff CA, Bock JJ, Buza V, Cheshire JR, Connors J, Cornelison J, Crumrine M, Cukierman AJ, Denison EV, Dierickx M, Duband L, Eiben M, Fatigoni S, Filippini JP, Goeckner-Wald N, Goldfinger D, Grayson JA, Grimes P, Hall G, Halpern M, Harrison SA, Henderson S, Hildebrandt SR, Hilton GC, Hubmayr J, Hui H, Irwin KD, Kang JH, Karkare KS, Kefeli S, Kovac JM, Kuo CL, Lau K, Leitch EM, Megerian KG, Minutolo L, Nakato Y, Namikawa T, Nguyen HT, O'brient R, Palladino S, Precup N, Prouve T, Pryke C, Racine B, Reintsema CD, Schillaci A, Schmitt BL, Soliman A, St. Germaine T, Steinbach B, Sudiwala RV, Thompson KL, Tucker C, Turner AD, Umlità C, Vieregg AG, Wandui A, Weber AC, Wiebe DV, Willmert J, Wu WLK, Yang E, Yoon KW, Young E, Yu C, Zeng L, Zhang C and Zhang S (2020), Dec., Receiver development for BICEP Array, a next-generation CMB polarimeter at the South Pole, Zmuidzinas J and Gao JR, (Eds.), *Millimeter, Submillimeter, and Far-Infrared Detectors and Instrumentation for Astronomy X*, Society of Photo-Optical Instrumentation Engineers (SPIE) Conference Series, 11453, pp. 1145314, 2012. 04047.
- Planck Collaboration, Aghanim N, Akrami Y, Ashdown M, Aumont J, Baccigalupi C, Ballardini M, Banday AJ, Barreiro RB, Bartolo N, Basak S, Benabed K, Bernard JP, Bersanelli M, Bielewicz P, Bock JJ, Bond JR, Borrill J, Bouchet FR, Boulanger F, Bucher M, Burigana C, Butler RC, Calabrese E, Cardoso JF, Carron J, Casaponsa B, Challinor A, Chiang HC, Colombo LPL, Combet C, Crill BP, Cuttaia F, de Bernardis P, de Rosa A, de Zotti G, Delabouille J, Delouis JM, Di Valentino E, Diego JM, Doré O, Douspis M, Ducout A, Dupac X, Dusini S, Efstathiou G, Elsner F, Enßlin TA, Eriksen HK, Fantaye Y, Fernandez-Cobos R, Finelli F, Frailis M, Fraisse AA, Franceschi E, Frolov A, Galeotta S, Galli S, Ganga K, Génova-Santos RT, Gerbino M, Ghosh T, Giraud-Héraud Y, González-Nuevo J, Górski KM, Gratton S, Gruppuso A, Gudmundsson JE, Hamann J, Handley W, Hansen FK, Herranz D, Hivon E, Huang Z, Jaffe AH, Jones WC, Keihänen E, Keskitalo R, Kiiveri K, Kim J, Kisner TS, Krachmalnicoff N, Kunz M, Kurki-Suonio H, Lagache G, Lamarre JM, Lasenby A, Lattanzi M, Lawrence CR, Le Jeune M, Levrier F, Lewis A, Liguori M, Lilje PB, Liddle M, Lindholm V, López-Cañiego M, Lubin PM, Ma YZ, Macías-Pérez JF, Maggio G, Maino D, Mandolesi N, Mangilli A, Marcos-Caballero A, Maris M, Martin PG, Martínez-González E, Matarrese S, Mauri N, McEwen JD, Meinhold PR, Melchiorri A, Mennella A, Migliaccio M, Millea M, Miville-Deschênes MA, Molinari D, Moneti A, Montier L, Morgante G, Moss A, Natoli P, Nørgaard-Nielsen HU, Pagano L, Paoletti D, Partridge B, Patanchon G, Peiris HV, Perrotta F, Pettorino V, Piacentini F, Polenta G, Puget JL, Rachen JP, Reinecke M, Remazeilles M, Renzi A, Rocha G, Rosset C, Roudier G, Rubiño-Martín JA, Ruiz-Granados B, Salvati L, Sandri M, Savelainen M, Scott D, Shellard EPS, Sirignano C, Sirri G, Spencer LD, Sunyaev R, Suur-Uski AS, Tauber JA, Tavagnacco D, Tenti M, Toffolatti L, Tomasi M, Trombetti T, Valiviita J, Van Tent B, Vielva P, Villa F, Vittorio N, Wandelt BD, Wehus IK, Zacchei A and Zonca A (2020a), Sep. Planck 2018 results. V. CMB power spectra and likelihoods. *A&A* 641, A5. doi:10.1051/0004-6361/201936386. 1907.12875.
- Planck Collaboration, Aghanim N, Akrami Y, Ashdown M, Aumont J, Baccigalupi C, Ballardini M, Banday AJ, Barreiro RB, Bartolo N, Basak S, Battye R, Benabed K, Bernard JP, Bersanelli M, Bielewicz P, Bock JJ, Bond JR, Borrill J, Bouchet FR, Boulanger F, Bucher M, Burigana C, Butler RC, Calabrese E, Cardoso JF, Carron J, Challinor A, Chiang HC, Chluba J, Colombo LPL, Combet C, Contreras D, Crill BP, Cuttaia F, de Bernardis P, de Zotti G, Delabouille J, Delouis JM, Di Valentino E, Diego JM, Doré O, Douspis M, Ducout A, Dupac X, Dusini S, Efstathiou G, Elsner F, Enßlin TA, Eriksen HK, Fantaye Y, Farhang M, Fergusson J, Fernandez-Cobos R, Finelli F, Forastieri F, Frailis M, Fraisse AA, Franceschi E, Frolov A, Galeotta S, Galli S, Ganga K, Génova-Santos RT, Gerbino M, Ghosh T, González-Nuevo J, Górski KM, Gratton S, Gruppuso A, Gudmundsson JE, Hamann J, Handley W, Hansen FK, Herranz D, Hildebrandt SR, Hivon E, Huang Z, Jaffe AH, Jones WC, Karakci A, Keihänen E, Keskitalo R, Kiiveri K, Kim J, Kisner TS, Knox L, Krachmalnicoff N, Kunz M, Kurki-Suonio H, Lagache G, Lamarre JM, Lasenby A, Lattanzi M, Lawrence CR, Le Jeune M, Lemos P, Lesgourgues J, Levrier F, Lewis A, Liguori M, Lilje PB, Liddle M, Lindholm V, López-Cañiego M, Lubin PM, Ma YZ, Macías-Pérez JF, Maggio G, Maino D, Mandolesi N, Mangilli A, Marcos-Caballero A, Maris M, Martin PG, Martinelli M, Martínez-González E, Matarrese S, Mauri N, McEwen JD, Meinhold PR, Melchiorri A, Mennella A, Migliaccio M, Millea M, Miville-Deschênes MA, Molinari D, Montier L, Morgante G, Moss A, Natoli P, Nørgaard-Nielsen HU, Pagano L, Paoletti D, Partridge B, Patanchon G, Peiris HV, Perrotta F, Pettorino V, Piacentini F, Polenta G, Puget JL, Rachen JP, Reinecke M, Remazeilles M, Renzi A, Rocha G, Rosset C, Roudier G, Rubiño-Martín JA, Ruiz-Granados B, Salvati L, Sandri M, Savelainen M, Scott D, Shellard EPS, Sirignano C, Sirri G, Spencer LD, Sunyaev R, Suur-Uski AS, Tauber JA, Tavagnacco D, Tenti M, Toffolatti L, Tomasi M, Trombetti T, Valenziano L, Valiviita J, Van Tent B, Vibert L, Vielva P, Villa F, Vittorio N, Wandelt BD, Wehus IK, White M, White SDM, Zacchei A and Zonca A (2020b), Sep. Planck 2018 results. VI. Cosmological parameters. *A&A* 641, A6. doi:10.1051/0004-6361/201833910. 1807.06209.
- Polarbear Collaboration, Ade PAR, Akiba Y, Anthony AE, Arnold K, Atlas M, Barron D, Boettger D, Borrill J, Chapman S, Chinone Y, Dobbs M, Elleflot T, Errard J, Fabbian G, Feng C, Flanagan D, Gilbert A, Grainger W, Halverson NW, Hasegawa M, Hattori K, Hazumi M, Holzapfel WL, Hori Y, Howard J, Hyland P, Inoue Y, Jaehnig GC, Jaffe AH, Keating B, Kermish Z, Keskitalo R, Kisner T, Le Jeune M, Lee AT, Leitch EM, Linder E, Lungu M, Matsuda F, Matsumura T, Meng X, Miller NJ, Morii H, Moyerman S, Myers MJ, Navaroli M, Nishino H, Orlando A, Paar H, Peloton J, Poletti D, Quealy E, Rebeiz G, Reichardt CL, Richards PL, Ross C, Schanning I, Schenck DE, Sherwin BD, Shimizu A, Shimmmin C, Shimon M, Siritanasak P, Smecher G, Spieler H, Stebor N, Steinbach B, Stompor R, Suzuki A, Takakura S, Tomaru T, Wilson B, Yadav A and Zahn O (2014), Oct. A Measurement of the Cosmic Microwave Background B-mode Polarization Power Spectrum at Sub-degree Scales with POLARBEAR. *ApJ* 794 (2), 171. doi:10.1088/0004-637X/794/2/171. 1403.2369.
- POLARBEAR Collaboration, Ade PAR, Aguilar M, Akiba Y, Arnold K, Baccigalupi C, Barron D, Beck D, Bianchini F, Boettger D, Borrill J, Chapman S, Chinone Y, Crowley K, Cukierman A, Dünner R, Dobbs M, Ducout A, Elleflot T, Errard J, Fabbian G, Feeney SM, Feng C, Fujino T, Galitzki N, Gilbert A, Goeckner-Wald N, Groh JC, Hall G, Halverson N, Hamada T, Hasegawa M, Hazumi M, Hill CA, Howe L, Inoue Y, Jaehnig G, Jaffe AH, Jeong O, Kaneko D, Katayama N, Keating B, Keskitalo R, Kisner T, Krachmalnicoff N, Kusaka A, Jeune ML, Lee AT, Leitch EM, Leon D, Linder E, Lowry L, Matsuda F, Matsumura T, Minami Y, Montgomery J, Navaroli M, Nishino H, Paar H, Peloton J, Pham ATP, Poletti D, Puglisi G, Reichardt CL, Richards PL, Ross C, Segawa Y, Sherwin BD, Silva-Feaver M, Siritanasak P, Stebor N, Stompor R, Suzuki A, Tajima O, Takakura S, Takatori S, Tanabe D, Teply GP, Tomaru T, Tucker C, Whitehorn N and Zahn A (2017), oct. A Measurement of the cosmic microwave background b-mode polarization power spectrum at subdegree scales from two years of polarbear data. *The Astrophysical Journal* 848 (2): 121. doi:10.3847/1538-4357/aa8e9f. <https://dx.doi.org/10.3847/1538-4357/aa8e9f>.
- Readhead ACS and Pearson TJ (2004), Jan., Interferometric Observations of the Cosmic Microwave Background Radiation, Freedman WL, (Ed.), *Measuring and Modeling the Universe*, pp. 349, astro-ph/0306383.
- Sayre JT, Reichardt CL, Henning JW, Ade PAR, Anderson AJ, Austermann JE, Avva JS, Beall JA, Bender AN, Benson BA, Bianchini F, Bleem LE, Carlstrom JE, Chang CL, Chaubal P, Chiang HC, Citron R, Corbett Moran C, Crawford TM, Crites AT, de Haan T, Dobbs MA, Everett W, Gallicchio J, George EM, Gilbert A, Gupta N, Halverson NW, Harrington N, Hilton GC, Holder GP, Holzapfel WL, Hrubes JD, Huang N, Hubmayr J, Irwin KD, Knox L, Lee AT, Li D, Lowitz A, McMahon JJ, Meyer SS, Mocuano LM, Montgomery J, Nadolski A, Natoli T, Nibarger JP, Noble G, Novosad V, Padin S, Patil S, Pryke C, Ruhl JE, Salwanchik BR, Schaffer KK, Sievers C, Smecher G, Stark AA, Tucker C,

- Vanderlinde K, Veach T, Vieira JD, Wang G, Whitehorn N, Wu WLK, Yefremenko V and SPTpol Collaboration (2020), Jun. Measurements of B -mode polarization of the cosmic microwave background from 500 square degrees of SPTpol data. *PRD* 101 (12), 122003. doi:10.1103/PhysRevD.101.122003. 1910.05748.
- Scott P (2023). The am atmospheric model. doi:10.5281/zenodo.640645.
- Scott D, Contreras D, Narimani A and Ma YZ (2016), Jun. The information content of cosmic microwave background anisotropies. *JCAP* 2016 (6), 046. doi:10.1088/1475-7516/2016/06/046. 1603.03550.
- Smith KM (2006), Oct. Pseudo- C_l estimators which do not mix E and B modes. *PRD* 74 (8), 083002. doi:10.1103/PhysRevD.74.083002. astro-ph/0511629.
- Sobrin JA, Anderson AJ, Bender AN, Benson BA, Dutcher D, Foster A, Goeckner-Wald N, Montgomery J, Nadolski A, Rahlin A, Ade PAR, Ahmed Z, Anderes E, Archipley M, Austermann JE, Avva JS, Aylor K, Balkenhol L, Barry PS, Thakur RB, Benabed K, Bianchini F, Bleem LE, Bouchet FR, Bryant L, Byrum K, Carlstrom JE, Carter FW, Cecil TW, Chang CL, Chaubal P, Chen G, Cho HM, Chou TL, Cliche JF, Crawford TM, Cukierman A, Daley C, de Haan T, Denison EV, Dibert K, Ding J, Dobbs MA, Everett W, Feng C, Ferguson KR, Fu J, Galli S, Gambrel AE, Gardner RW, Gualtieri R, Guns S, Gupta N, Guysier R, Halverson NW, Harke-Hosemann AH, Harrington NL, Henning JW, Hilton GC, Hivon E, Holder GP, Holzapfel WL, Hood JC, Howe D, Huang N, Irwin KD, Jeong OB, Jonas M, Jones A, Khaire TS, Knox L, Kofman AM, Korman M, Kubik DL, Kuhlmann S, Kuo CL, Lee AT, Leitch EM, Lowitz AE, Lu C, Meyer SS, Michalik D, Millea M, Natoli T, Nguyen H, Noble GI, Novosad V, Omori Y, Padin S, Pan Z, Paschos P, Pearson J, Posada CM, Prabhu K, Quan W, Reichardt CL, Riebel D, Riedel B, Rouble M, Ruhl JE, Saliwanchik B, Sayre JT, Schiappucci E, Shirokoff E, Smecher G, Stark AA, Stephen J, Story KT, Suzuki A, Tandoi C, Thompson KL, Thorne B, Tucker C, Umlita C, Vale LR, Vanderlinde K, Vieira JD, Wang G, Whitehorn N, Wu WLK, Yefremenko V, Yoon KW and Young MR (2022), feb. The design and integrated performance of spt-3g. *The Astrophysical Journal Supplement Series* 258 (2): 42. doi:10.3847/1538-4365/ac374f. <https://dx.doi.org/10.3847/1538-4365/ac374f>.
- Sobrin JA, Anderson AJ, Bender AN, Benson BA, Dutcher D, Foster A, Goeckner-Wald N, Montgomery J, Nadolski A, Rahlin A, Ade PAR, Ahmed Z, Anderes E, Archipley M, Austermann JE, Avva JS, Aylor K, Balkenhol L, Barry PS, Thakur RB, Benabed K, Bianchini F, Bleem LE, Bouchet FR, Bryant L, Byrum K, Carlstrom JE, Carter FW, Cecil TW, Chang CL, Chaubal P, Chen G, Cho HM, Chou TL, Cliche JF, Crawford TM, Cukierman A, Daley C, de Haan T, Denison EV, Dibert K, Ding J, Dobbs MA, Everett W, Feng C, Ferguson KR, Fu J, Galli S, Gambrel AE, Gardner RW, Gualtieri R, Guns S, Gupta N, Guysier R, Halverson NW, Harke-Hosemann AH, Harrington NL, Henning JW, Hilton GC, Hivon E, Holder GP, Holzapfel WL, Hood JC, Howe D, Huang N, Irwin KD, Jeong OB, Jonas M, Jones A, Khaire TS, Knox L, Kofman AM, Korman M, Kubik DL, Kuhlmann S, Kuo CL, Lee AT, Leitch EM, Lowitz AE, Lu C, Meyer SS, Michalik D, Millea M, Natoli T, Nguyen H, Noble GI, Novosad V, Omori Y, Padin S, Pan Z, Paschos P, Pearson J, Posada CM, Prabhu K, Quan W, Reichardt CL, Riebel D, Riedel B, Rouble M, Ruhl JE, Saliwanchik B, Sayre JT, Schiappucci E, Shirokoff E, Smecher G, Stark AA, Stephen J, Story KT, Suzuki A, Tandoi C, Thompson KL, Thorne B, Tucker C, Umlita C, Vale LR, Vanderlinde K, Vieira JD, Wang G, Whitehorn N, Wu WLK, Yefremenko V, Yoon KW and Young MR (2022), Feb. The Design and Integrated Performance of SPT-3G. *ApJS* 258 (2), 42. doi:10.3847/1538-4365/ac374f. 2106.11202.
- Suzuki A, Ade P, Akiba Y, Aleman C, Arnold K, Baccigalupi C, Barch B, Barron D, Bender A, Boettger D, Borrill J, Chapman S, Chinone Y, Cukierman A, Dobbs M, Ducout A, Dunner R, Elleflot T, Errard J, Fabbian G, Feeney S, Feng C, Fujino T, Fuller G, Gilbert A, Goeckner-Wald N, Groh J, Haan TD, Hall G, Halverson N, Hamada T, Hasegawa M, Hattori K, Hazumi M, Hill C, Holzapfel W, Hori Y, Howe L, Inoue Y, Irie F, Jaehnig G, Jaffe A, Jeong O, Katayama N, Kaufman J, Kazemzadeh K, Keating B, Kermish Z, Keskitalo R, Kisner T, Kusaka A, Jeune ML, Lee A, Leon D, Linder E, Lowry L, Matsuda F, Matsumura T, Miller N, Mizukami K, Montgomery J, Navaroli M, Nishino H, Peloton J, Poletti D, Puglisi G, Rebeiz G, Raum C, Reichardt C, Richards P, Ross C, Rotermund K, Segawa Y, Sherwin B, Shirley I, Siritanasak P, Stebor N, Stompor R, Suzuki J, Tajima O, Takada S, Takakura S, Takatori S, Tikhomirov A, Tomaru T, Westbrook B, Whitehorn N, Yamashita T, Zahn A and Zahn O (2016), Aug. The Polarbear-2 and the Simons Array Experiments. *Journal of Low Temperature Physics* 184 (3-4): 805–810. doi:10.1007/s10909-015-1425-4. 1512.07299.
- Takakura S, Aguilar-Faúndez MAO, Akiba Y, Arnold K, Baccigalupi C, Barron D, Beck D, Bianchini F, Boettger D, Borrill J, Cheung K, Chinone Y, Elleflot T, Errard J, Fabbian G, Feng C, Goeckner-Wald N, Hamada T, Hasegawa M, Hazumi M, Howe L, Kaneko D, Katayama N, Keating B, Keskitalo R, Kisner T, Krachmalnicoff N, Kusaka A, Lee AT, Lowry LN, Matsuda FT, May AJ, Minami Y, Navaroli M, Nishino H, Piccirillo L, Poletti D, Puglisi G, Reichardt CL, Segawa Y, Silva-Feaver M, Siritanasak P, Suzuki A, Tajima O, Takatori S, Tanabe D, Tepy GP and Tsai C (2019), Jan. Measurements of Tropospheric Ice Clouds with a Ground-based CMB Polarization Experiment, POLARBEAR. *ApJ* 870 (2), 102. doi:10.3847/1538-4357/aaf381. 1809.06556.
- Ulbricht G, De Lucia M and Baldwin E (2021). Applications for microwave kinetic induction detectors in advanced instrumentation. *Applied Sciences* 11 (6). ISSN 2076-3417. doi:10.3390/app11062671. <https://www.mdpi.com/2076-3417/11/6/2671>.
- Zaldarriaga M (2001). Nature of the e-b decomposition of cmb polarization. *Physical Review D* 64: 103001. ISSN 1550-79980556-2821. doi:10.1103/PhysRevD.64.103001. <https://ui.adsabs.harvard.edu/abs/2001PhRvD..64j3001Z>, Journal Article.